ORIGINAL ARTICLE

Toluidine Blue-Loaded Nanomicelles for Photodynamic Therapy of Lung Cancer: An In-vitro Study

Bahareh Khalili Najafabad [1*], Mehdi Hoseini [2,3], Amirhossein Rashnoodi [1], Saleh Rouhi [4], Soroush Najafisarvestani [5], Zeynab Seraj [1], Ghazal Sadraei [1]

[1] *Department of Biomedical Engineering and Medical physics, Shahid Beheshti University of Medical Sciences, Tehran, Iran*

[2] *Department of Radiology Technology, School of Paramedical Sciences, Torbat Heydariyeh University of Medical Sciences, Torbat Heydariyeh, Iran*

[3] *Research Center of Advanced Technologies in Medicine, Torbat Heydariyeh University of Medical Sciences, Torbat Heydariyeh, Iran*

[4] *Department of Medical Physics, Faculty of Medicine, Kermanshah University of Medical Sciences, Kermanshah, Iran*

[5] *Department of Medical Physics, School of Medicine, Shahid Sadoughi University of Medical Sciences, Yazd, Iran*

*Corresponding Author: Bahareh Khalili Najafabad
Email: luxinguo577@gmail.com

Received: 23 June 2026 / Accepted: 19 August 2026

Abstract

Purpose: Photodynamic Therapy (PDT) has attracted considerable attention as a non-invasive and selective method for cancer treatment. In this study, the photodynamic effects of Nanomicelles (NMs) loaded with the dye Toluidine Blue (TB) were evaluated on human lung cancer (QU-DB) and non-cancerous (MRC-5) cell lines. NMs, as biocompatible carriers, possess the ability to improve solubility, stability, and targeted accumulation of a photosensitizer (PS), while showing enhanced tumor tissue accumulation through the enhanced permeability and retention (EPR) effect.

Materials and Methods: The TB-loaded NMs were synthesized using the direct dissolution method and underwent physicochemical characterization. Then, cells were irradiated with laser red light ($\lambda = 655$ nm) at doses of 10, 20, and 40 J/cm^2. Post-irradiation, cell viability was quantified via the MTT assay, enabling the calculation of key therapeutic indices such as IC_{50}, ED_{50}, and the Synergy Index (SI).

Results: The results demonstrated that encapsulating TB in NMs increased optical absorption, reduced dye aggregation, and consequently enhanced reactive oxygen species (ROS) generation efficiency. The photodynamic effect of TB-loaded NMs was significantly stronger in the QU-DB cancer cell line compared with free TB, while inducing lower toxicity in the non-tumor MRC-5 cells. Thus, the selective distinction between tumor and non-cancerous cell lines was confirmed. Furthermore, increasing light dose resulted in greater cytotoxicity, with dose-dependent reductions in cell survival. However, no favorable selectivity index was obtained when comparing micellar drug cytotoxicity with the free PS ($p > 0.05$).

Conclusion: TB-loaded NMs represent a promising drug delivery system to enhance the efficacy and selectivity of PDT in lung cancer while reducing its off-target effects.

Keywords: Photodynamic Therapy; Toluidine Blue; Nanomicelles; Lung Cancer; Selective Cytotoxicity.

DOI:

1. Introduction

Lung cancer is one of the most significant global health challenges of the 21st century, responsible for many deaths annually, especially in industrialized countries [1, 2]. Despite major advances in surgery, chemotherapy, and radiotherapy, current treatments are still limited by non-selectivity, systemic toxicity, and the emergence of resistance mechanisms in tumorigenic cells [3]. Consequently, there has been growing interest in developing targeted, minimally invasive therapeutic modalities that can selectively eradicate cancer cells while sparing normal tissues, one such approach that has gained increasing attention is Photodynamic Therapy (PDT) [4].

PDT is a photo-oxidative process requiring three essential components: a Photosensitizer (PS), light of a specific wavelength, and molecular oxygen [5]. Following light activation, the PS transitions to an excited singlet state, then undergoes intersystem crossing to a longer-lived triplet state [6]. From this triplet state, it can generate Reactive Oxygen Species (ROS), primarily singlet oxygen ($^1O_2$), via energy transfer to molecular oxygen [7]. These ROS induce oxidative stress in biological molecules, including lipids, proteins, and nucleic acids, ultimately cause irreversible damage and cell death through apoptosis, necrosis, or autophagy [8]. As a minimally invasive and repeatable procedure, PDT's primary advantage lies in its precise spatial controllability; the cytotoxic effect is confined exclusively to the irradiated area where the PS accumulated, thereby selectively eradicating diseased cells while sparing adjacent healthy tissue [9].

Among the different classes of PSs, Toluidine Blue (TB), which is a cationic thiazine dye, has been widely studied for PDT applications due to its strong absorption in the red region (around 630-660 nm), high singlet oxygen quantum yield, and low dark toxicity [10]. TB also exhibits selective binding to negatively charged cellular components such as DNA and phospholipids, making it particularly effective in targeting malignant cells that often possess higher membrane potential and a more acidic microenvironment [11]. However, the clinical utility of second-generation PSs like TB remains restricted because of several physicochemical limitations, including the tendency to aggregate in aqueous solutions, which directly impairs its cellular uptake and ultimately diminishes the therapeutic efficiency of PDT [12].

To overcome these challenges, nanotechnology has emerged as a powerful and versatile platform that not only improves the delivery and performance of Photosensitizing drugs (PS) but also opens new horizons in the fields of diagnosis [13, 14] and therapy [15-17]. Nanocarriers provide the ability to deliver drugs to tumor tissue, enhance contrast in medical imaging, and even improve the efficacy of radiotherapy [18-20]. Among these nanocarriers, nanomicelles (NMs) occupy a special place due to their remarkable ability to improve solubility, increase photostability, and induce selective accumulation in tumor tissue [21]. These self-assembled colloidal structures, usually composed of amphiphilic surfactants, have a core-shell architecture: a hydrophobic core to encapsulate poorly soluble drugs and a hydrophilic shell that ensures stability in aqueous environments and stealth properties (non-recognition by the immune system) [22]. Their nanoscale size (typically 1–100 nm) allows for preferential tumor accumulation through the Enhanced Permeability and Retention (EPR) effect, a phenomenon that results from leaky blood vessels and impaired lymphatic drainage of solid tumors [23].

In this regard, the present study focuses on the synthesis and evaluation of TB-containing NMs formulated with nonionic surfactants Tween-80 and Span-80, the combination of which allows for precise control of the micelle Hydrophilic-Lipophilic Balance (HLB), thereby improving TB encapsulation and stability (15). This nanomicelle system is expected to facilitate selective delivery to tumorigenic cells by preventing TB aggregation, protecting against photobleaching, and providing sustained release. In this study, we have investigated the photodynamic performance of TB-containing NMs on two human lung cell lines, including the QU-DB cancer cell line and the MRC-5 normal fibroblast cell line. This study was conducted to evaluate the physicochemical properties of the NMs, optimize the light irradiation parameters, and evaluate the cytotoxic effects under dark and light conditions, through a systematic experimental design. The broader goal of this research is to determine whether micellar encapsulation of TB can enhance its therapeutic efficacy and reduce

damage to non-malignant cells, ultimately providing a basis for novel nanocarrier-based PDT strategies in the treatment of lung cancer.

2. Materials and Methods

2.1. Chemicals and Materials

TB was employed as the primary PS throughout this study. The non-ionic surfactants Tween-80 (hydrophilic) and Span-80 (lipophilic), both purchased from Merck Chemicals (Darmstadt, Germany), were utilized as amphiphilic agents for nanomicelle fabrication. These particular surfactants were selected based on their well-established biocompatibility, FDA approval status, and complementary hydrophilic-lipophilic balance (HLB) values of 15.0 for Tween-80 and 4.3 for Span-80, which collectively enabled precise tuning of the micellar system's overall HLB and stability. Additional reagents included dimethyl sulfoxide (DMSO) as a solvent, phosphate-buffered saline (PBS) for washing procedures, and Dulbecco's Modified Eagle Medium (DMEM) supplemented with 10% fetal bovine serum (FBS) and 1% penicillin-streptomycin for cell culture maintenance. All chemicals were of analytical grade and were used as received without further purification.

2.2. Synthesis of TB-Loaded NMs

The TB-loaded NMs were prepared using a straightforward direct dissolution method. Briefly, a 50 µg/mL solution of TB was first prepared in distilled deionized water at pH 5.6. The surfactants Tween-80 (hydrophilic) and Span-80 (lipophilic) were then combined in a 60:40 molar ratio to achieve an overall HLB value of 8.85, which was previously determined to be optimal for stable micelle formation. This surfactant mixture was subsequently added to the TB solution and subjected to continuous magnetic stirring at 1000 rpm for 2 hours at 30°C using a 25 mm magnetic stir bar, while the pH was carefully maintained at 5.6 throughout the process using phosphate buffer. Under these optimized conditions, NMs spontaneously self-assembled, with final concentrations adjusted to 1.5 mM Tween-80 and 1.0 mM Span-80 (60:40 molar ratio) [24]. Following synthesis, the formulation was filtered through a 0.22 µm PES membrane to remove unencapsulated free dye and any unassembled surfactant residues. The prepared NMs were stored in amber glass vials at 4°C to prevent photodegradation and minimize aggregation, and were subsequently characterized for particle size distribution, optical properties, and encapsulation efficiency within 24 hours of preparation [25].

2.3. Physicochemical Characterization

The physicochemical properties of the synthesized NMs were comprehensively evaluated through multiple complementary techniques. Dynamic Light Scattering (DLS) was employed to determine the hydrodynamic diameter and polydispersity index (PDI) of the formulations, with samples appropriately diluted at a 1:30 ratio prior to measurement [26]. The optical absorption spectra of both TB-loaded NMs and free TB solutions (at equivalent dye concentrations) were recorded using a UV-Vis spectrophotometer, and the characteristic absorbance peaks were analyzed to assess dye encapsulation efficiency and aggregation behavior. Zeta potential measurements were performed using a Zetasizer Nano ZS (Malvern Instruments, UK) at 25°C. Samples were diluted 1:30 with deionized water and measured in disposable folded capillary cells (DTS1070). Three measurements were taken for each sample, with each measurement consisting of at least 10 runs. The zeta potential of TB-loaded nanomicelles was determined to be -18.5 ± 2.1 mV at pH 7.4, indicating moderate colloidal stability through electrostatic repulsion. The physical stability of the formulation was evaluated over a two-week period by monitoring absorbance decay and turbidity changes under dark storage conditions at 25°C, in comparison with free TB control samples. Encapsulation efficiency (EE%) was calculated according to the standard formula: EE% = (Practical Loading / Theoretical Loading) × 100, which yielded a representative value of approximately 50%, indicating that half of the initial TB was successfully entrapped within the micellar core. Additionally, the photostability of TB was assessed by exposing both micellar and free TB samples to three clinically relevant irradiation doses (10, 20, and 40 J/cm²) using a 655 nm diode laser, with absorption spectra recorded immediately before and after each

irradiation session to quantify any photobleaching effects.

2.4. Cell Lines and Culture Conditions

Two distinct human lung cell lines were selected for the in vitro experiments: the QU-DB large-cell lung carcinoma line (as a tumorigenic model) and the MRC-5 normal human lung fibroblast line (as a non-tumorigenic control). Both cell lines were obtained from the cell bank of the Pasteur Institute of Iran (Tehran, Iran) and were routinely maintained in DMEM medium supplemented with 10% heat-inactivated fetal bovine serum, 1% penicillin, and 1% streptomycin. Cells were cultured in a humidified incubator at 37°C with 5% CO_2 atmosphere and were passaged upon reaching approximately 80% confluence. For the cytotoxicity and PDT assays, cells were seeded into 96-well microplates at a density of 3.5×10^4 cells per well and allowed to adhere for 24 hours prior to treatment [27]. For photodynamic experiments, cells were irradiated with a continuous-wave diode laser emitting at 655 nm, with energy densities of 10, 20, and 40 J/cm² applied to designated treatment groups, while control groups were maintained under identical conditions without light exposure. Following irradiation, cells were returned to the incubator for an additional 24 hours, after which cell viability was assessed using the standard MTT colorimetric assay. Briefly, MTT reagent (3-(4,5-dimethylthiazol-2-yl)-2,5-diphenyltetrazolium bromide) was added to each well and incubated for 4 hours, allowing the formation of purple formazan crystals, which were subsequently dissolved in DMSO. The optical density of each well was then measured at 570 nm using a microplate reader, with absorbance values directly correlating to the number of viable cells.

2.5. Illumination Protocol

The illumination procedure was carefully standardized to ensure reproducibility across all PDT experiments. Both QU-DB and MRC-5 cell lines were subjected to three different light doses (10, 20, and 40 J/cm²) delivered by a 655 nm continuous-wave diode laser system. The laser output was calibrated prior to each experiment using a power meter to ensure accurate energy delivery, and the beam was uniformly expanded to cover the entire surface area of each well in the 96-well plate. Treatment groups receiving the same drug concentration were irradiated in parallel to minimize experimental variability. Following laser exposure, cells were immediately returned to the incubator and maintained under standard culture conditions for 24 hours, after which the photodynamic efficacy was quantitatively evaluated using the MTT assay as described above. Dark toxicity controls were also included, in which cells were treated with identical drug concentrations but were kept in complete darkness throughout the entire experimental period.

2.6. Statistical Analysis

All experiments were performed in triplicate to ensure reproducibility and statistical reliability, with results expressed as mean ± standard deviation (SD). Statistical significance between experimental groups was evaluated using one-way analysis of variance (ANOVA), followed by Tukey's post hoc test for multiple group comparisons. A p-value of less than 0.05 was considered statistically significant for all analyses. The selectivity index (SI) was calculated as the ratio of IC_{50} values in normal cells to IC_{50} values in cancer cells, where $SI > 2$ was considered indicative of favorable selectivity. Synergy indices between light and drug treatments were calculated to evaluate potential cooperative effects. All statistical computations were performed using SPSS software version 22.0 (IBM Corp., Armonk, NY, USA), and graphical representations were generated using GraphPad Prism version 8.0 (GraphPad Software, La Jolla, CA, USA).

3. Results

3.1. Physical Stability

3.1.1. Spectrophotometric Analysis

The physical stability of free TB and TB-loaded NMs was evaluated over 14 days using UV-Vis spectrophotometry at four concentrations (1, 5, 10, and 25 µg/mL) on days 1, 7, and 14 (Figure 1). The micellar formulation demonstrated significantly enhanced stability compared with free TB. Over the two-week period, the absorbance peak of free TB declined by approximately 54%, whereas TB-loaded

NMs exhibited a substantially lower decrease of approximately 31%, representing a 23% improvement in physical stability conferred by nanomicellar encapsulation. These findings confirm that the micellar microenvironment effectively protects TB from aggregation and degradation, preserving its optical properties over time.

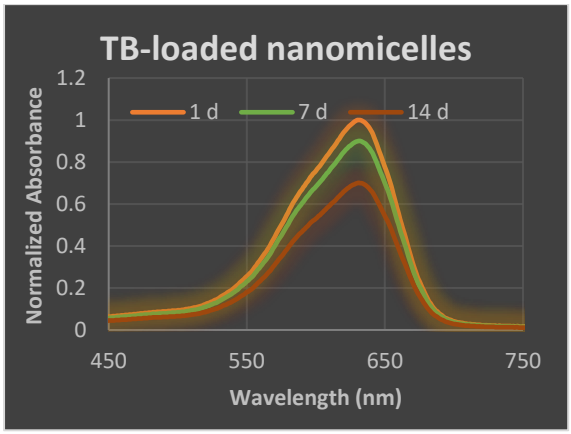

a

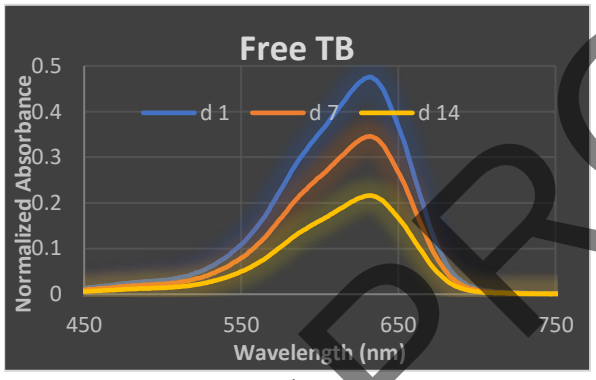

b

Figure 1. Absorption spectra of TB-loaded nanomicelles (a) and free TB (b) samples in first, seventh and fourteenth day of synthesis

3.1.2. DLS Analysis

Particle size distribution and PDI of TB-loaded NMs were characterized by DLS on days 1 and 14 (Figure 2). On the first day, the formulation exhibited a favorable size distribution in the 40–120 nm range with a peak at approximately 70–87 nm, which is advantageous for EPR-mediated tumor accumulation and cellular uptake. After two weeks, a visible shift toward larger particle sizes and broadening of the distribution curve were observed, indicating some aggregation over time. The PDI increased from 0.214 on day 1 to 0.346 on day 14, confirming the broadening of size distribution. Despite this gradual change, the most prevalent size range remained within acceptable limits for PDT applications.

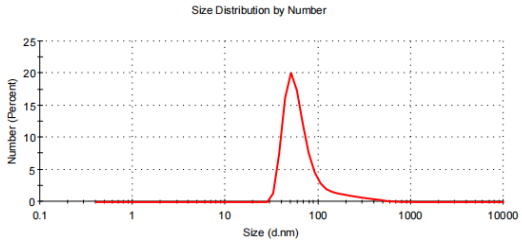

a

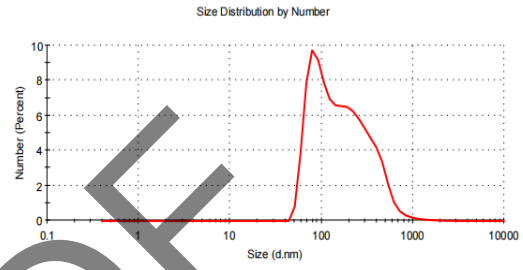

b

Figure 2. DLS results for the loaded sample in the first (a) and 14th (b) day of synthesis, the first day distribution in sample volume exhibits a 40-120 nm size range with a peak around 70 nm and in 14th day, there is a visible increase in width of distribution curve which can be attributed to aggregation of particles in time

3.2. Photo-Stability Findings

The photostability of free TB and TB-loaded NMs was evaluated by exposing samples to three therapeutic light doses (10, 20, and 40 J/cm²) using a 655 nm diode laser. Absorption spectra recorded before and after irradiation revealed no meaningful differences between micellar and free samples upon increasing light dose, indicating minimal photobleaching for both formulations. This remarkable photostability ensures consistent ROS generation throughout the irradiation period, simplifying treatment planning and potentially allowing for reduced drug doses to achieve equivalent therapeutic effects.

3.3. Dark Toxicity

The dark toxicity of free TB and TB-loaded NMs was assessed using MTT assay in both QU-DB cancer and MRC-5 normal cell lines (Figure 3). Statistical

analysis (ANOVA, $\alpha = 0.05$) revealed no significant differences in cell viability between treated groups and untreated controls for either formulation or cell line ($p > 0.05$). Additionally, no significant differences were observed between free and micellar forms in either cell type ($p > 0.05$). Notably, a slight increase in cell viability was observed for the micellar formulation in QU-DB cells, which can be attributed to the delayed and gradual release profile of the drug during the 1-hour incubation period. These results confirm the excellent biocompatibility of both formulations prior to light activation.

3.4. PDT Efficacy

3.4.1. Cytotoxicity in Non-Tumorigenic MRC-5 Cells

The photodynamic efficacy of free TB and TB-loaded NMs was evaluated in MRC-5 normal lung fibroblasts following exposure to 10, 20, and 40 J/cm² (Figure 4). Cell viability decreased in a concentration- and light dose-dependent manner for both formulations, with statistically significant reductions observed upon increasing drug concentration and irradiation dose ($p < 0.05$). The TB-loaded NMs demonstrated comparable or slightly higher phototoxicity than free TB at all light doses.

However, overall phototoxicity in MRC-5 cells remained relatively attenuated compared with that

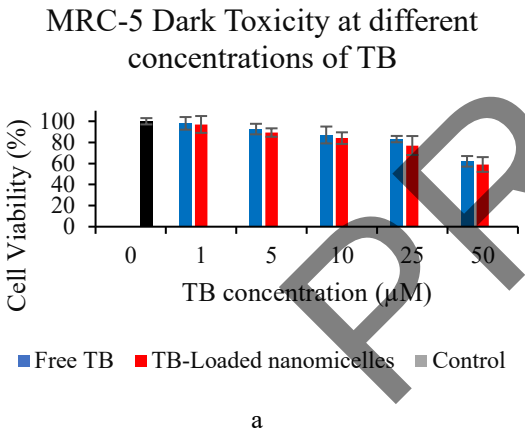

a

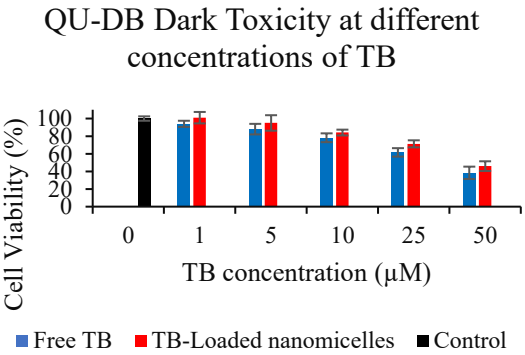

b

Figure 3. MTT results of dark toxicity of both loaded and free forms of the PS for both non-tumorigenic (a) and tumorigenic cell lines (b)

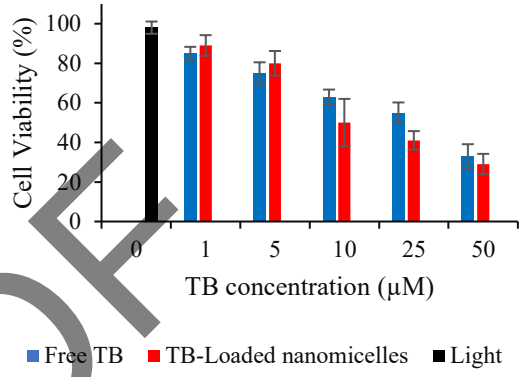

a

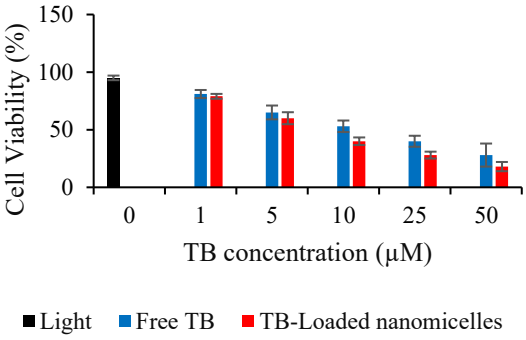

b

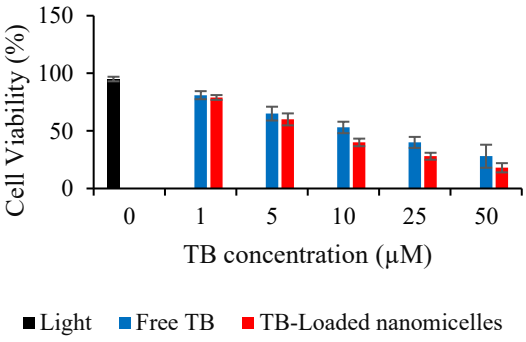

c

Figure 4. MTT results of the non-tumorigenic cell line for both free and loaded forms of the PS in three light doses of 10 (a), 20 (b) and 40 (c) J/cm²

observed in cancer cells, confirming acceptable safety margins for therapeutic applications.

3.4.2. Cytotoxicity in Tumorigenic QU-DB Cells

The photodynamic efficacy was further evaluated in QU-DB lung cancer cells under identical conditions (Figure 5). The results demonstrated a statistically significant increase in potency of the micellar formulation compared with free TB across all light doses, particularly at medium and higher drug concentrations ($p < 0.05$). At 40 J/cm², the most substantial differences were observed, with TB-loaded NMs achieving near-complete cell killing at higher concentrations. This enhanced potency is attributed to improved cellular uptake, reduced aggregation, and consequently greater ROS generation within cancer cells. The differential response between QU-DB and MRC-5 cells confirms the selective therapeutic potential of the nanomicellar system.

3.5. Quantitative Therapeutic Indices

IC_{50} values were determined for both cell lines and formulations across all light doses (Table 1). In QU-DB cells, IC_{50} values for TB-loaded NMs were consistently lower than those for free TB at all light doses, with the most pronounced difference at 40 J/cm² (4.1 ± 0.2 µM vs. 6.8 ± 0.4 µM). In MRC-5 cells, IC_{50} values were generally higher than in cancer cells, confirming selective toxicity. Both formulations exhibited relatively high IC_{50} values in dark conditions, confirming low intrinsic toxicity.

Table 1. Calculated IC50s for both cell lines and drug forms in three light doses

Formulation	Light Dose (J/cm²)	QU-DB (µM)	MRC-5 (µM)
Free TB	0 (Dark)	37.6 ± 1.6	67.3 ± 3.3
	10	28.1 ± 2.1	30.1 ± 1.8
	20	14.6 ± 0.8	21.2 ± 1.6
	40	6.8 ± 0.4	17.8 ± 0.6
TB-Loaded Nanomicelles	0 (Dark)	44.9 ± 2.2	60.8 ± 2.9
	10	26.4 ± 1.4	23.5 ± 1.5
	20	11.8 ± 0.6	14.6 ± 1.2
	40	4.1 ± 0.2	10.2 ± 0.4

Synergy indices were calculated to evaluate cooperative interactions between light and each formulation (Tables 2 and 3). In QU-DB cells, synergy indices increased with both drug concentration and light dose for both formulations. TB-loaded NMs consistently exhibited higher synergy indices than free TB, with the highest value of 3.1 observed at 20 J/cm² and 50 µM. Mean synergy indices for micellar formulations were 1.5 ± 0.4, 2.0 ± 0.8, and 2.1 ± 0.6 at 10, 20, and 40 J/cm², respectively, compared with 1.4 ± 0.2, 1.6 ± 0.4, and 1.7 ± 0.3 for free TB. Similarly, in MRC-5 cells, the micellar formulation demonstrated higher synergy indices than free TB, with mean values of 1.3 ± 0.06, 1.9 ± 0.4, and 2.3 ±

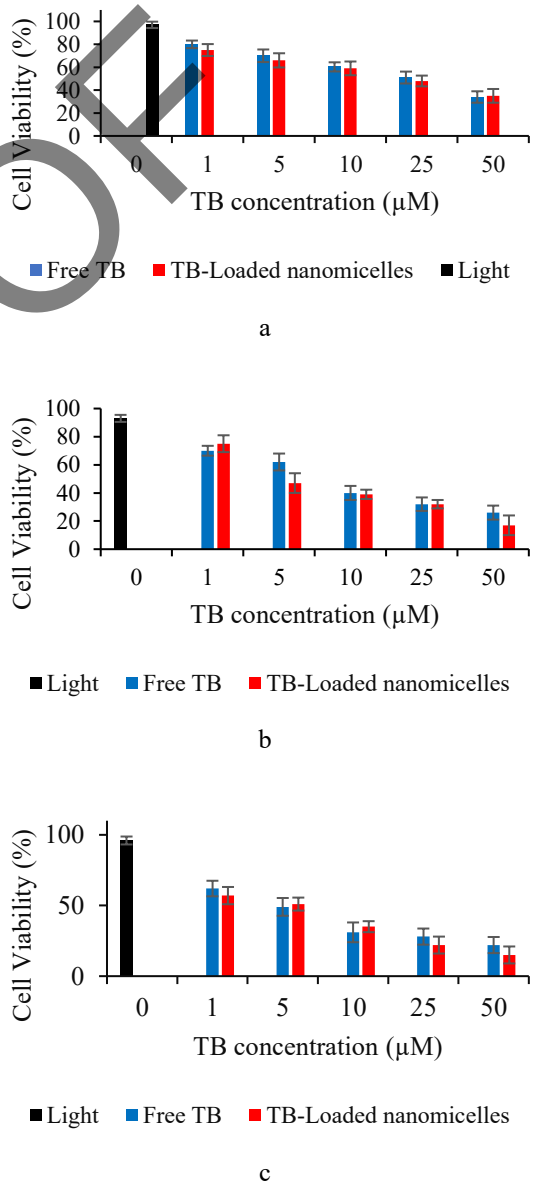

Figure 5. Viability of QU-DB cells treated with the free TB and TB-loaded nanomicelles at light doses of (a) 10, (b) 20, and (c) 40 J/cm²

Table 2. Synergy indexes of different concentration of drug in three light doses for the non- tumorigenic cell line

Drug Concentration (μM)	10 J/cm²		20 J/cm²		40 J/cm²	
	Free TB	TB-loaded nanomicelle	Free TB	TB-loaded nanomicelle	Free TB	TB-loaded nanomicelle
1	1.1	1.0	1.1	1.1	1.2	1.3
5	1.2	1.0	1.3	1.4	1.4	1.8
10	1.3	1.6	1.5	1.9	1.7	2.3
25	1.4	1.8	1.9	2.6	2.2	2.8
50	1.8	1.9	2.1	3.1	1.9	2.4
Mean ± Std	1.4 ± 0.2	1.5 ± 0.4	1.6 ± 0.4	2.0 ± 0.8	1.7 ± 0.3	2.1 ± 0.6

Table 3. Synergy indexes of different concentration of drug in three light doses for the non- tumorigenic cell line.

Drug Concentration (μM)	10 J/cm²		20 J/cm²		40 J/cm²	
	Free TB	TB-loaded nanomicelle	Free TB	TB-loaded nanomicelle	Free TB	TB-loaded nanomicelle
1	1.1	1.0	1.1	1.1	1.2	1.3
5	1.2	1.0	1.3	1.4	1.4	1.8
10	1.3	1.6	1.5	1.9	1.7	2.3
25	1.4	1.8	1.9	2.6	2.2	2.8
50	1.8	1.9	2.1	3.1	1.9	2.4
Mean ± Std	1.4 ± 0.2	1.5 ± 0.4	1.6 ± 0.4	2.0 ± 0.8	1.7 ± 0.3	2.1 ± 0.6

0.6 at 10, 20, and 40 J/cm², respectively, compared with 1.1 ± 0.06, 1.5 ± 0.2, and 1.8 ± 0.3 for free TB.

ED_{50} values were interpolated using a four-parameter logistic model (Figure 6). The analysis revealed that TB-loaded NMs required significantly lower global drug concentrations to achieve 50% cell killing compared with free TB in both cell lines, further confirming the enhanced therapeutic efficiency conferred by nanomicellar encapsulation. This reduction in effective dose suggests that lower drug doses may be sufficient to achieve equivalent therapeutic outcomes, potentially reducing systemic toxicity in clinical applications.

4. Discussion

The present study demonstrates that encapsulating TB within NMs significantly enhances its photodynamic performance in ways that are both physicochemically and biologically meaningful ($p < 0.05$). Spectroscopically, micellar loading effectively increased usable optical absorption and mitigated the inherent self-aggregation tendency of TB molecules in aqueous environments. Functionally, this improved physicochemical profile translated to markedly higher photodynamic potency against the tumorigenic QU-DB lung cancer cell line compared with free TB, while concurrently producing lower dark and light cytotoxicity in the non-tumorigenic MRC-5 lung fibroblast cell line. Cell viability decreased monotonically with increasing light dose (10, 20, and 40 J/cm²), confirming a clear dose-response relationship under red illumination at 655 nm. These findings collectively indicate that the nanomicellar

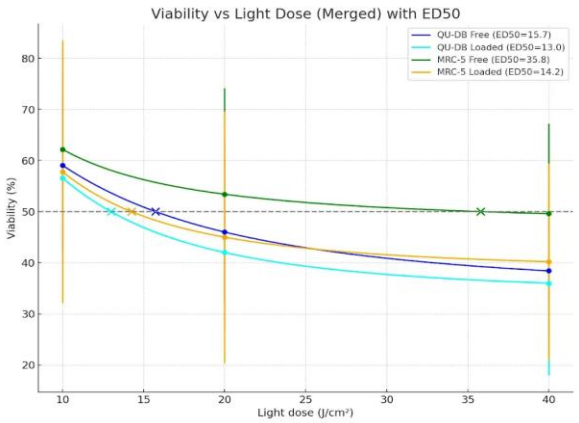

Figure 6. Interpolated ED50s for global concentration of the drug for both cell lines using 4 parameters logistic model

formulation successfully enhances the therapeutic window of TB-mediated PDT. Notably, although selectivity at the level of cell viability clearly favored QU-DB over MRC-5, an overall selectivity index advantage of the micellar formulation versus free TB did not reach statistical significance ($p = 0.22$), suggesting that while the formulation improves tumor cell killing, the differential selectivity requires further optimization.

4.1. Physicochemical Stability and Nano-Scale Attributes

The observed biological effects are strongly supported by the formulation's favorable stability profile and nano-scale architectural attributes. DLS analysis revealed a primary particle population centered around approximately 100 nm, which is consistent with expectations for carriers capable of exploiting the EPR effect for passive tumor targeting [28]. Over a two-week storage period, TB-loaded NMs retained their structural integrity with only modest broadening of the size distribution, whereas free TB exhibited more pronounced spectral drift arising from progressive aggregation. Correspondingly, the normalized absorbance peak of TB-loaded NMs declined by approximately 31% across two weeks, compared with roughly 54% for free TB. This relative preservation of chromophore function provides a physicochemical rationale for the improved photodynamic output observed after incubation and handling procedures. Furthermore, both free TB and micellar TB demonstrated minimal photobleaching across the therapeutic irradiation range of 10–40 J/cm², indicating that treatment-limiting dye degradation did not serve as a confounding factor in the observed cytotoxic differences between the two formulations. This photostability is particularly advantageous for PDT applications, as it ensures consistent ROS generation throughout the irradiation period and simplifies treatment planning calculations.

4.2. Dose-Response Relationships and Synergistic Effects

The dose-response analyses further elucidate a synergistic interaction between light and the micellar PS in the tumor setting. As light dose increased, the viability curves for QU-DB cells shifted downward more steeply with TB-loaded NMs than with free TB, a pattern consistent with enhanced intracellular delivery and consequently elevated ROS generation from the better-dispersed chromophore. By contrast, MRC-5 cells showed comparatively attenuated killing under identical experimental conditions, reinforcing the existence of a therapeutically favorable window for the micellar formulation [7]. The study's quantitative metrics, including IC_{50} (inhibitory concentration), ED_{50} (effective dose) derived from a four-parameter logistic model, and the combination (synergy) index, collectively capture this pattern: stronger light-drug interaction in QU-DB cells than in MRC-5 cells, which aligns with the formulation's intended purpose of amplifying PDT efficacy precisely where tumor biology and micellar uptake intersect [24]. The synergy indexes calculated for both cell lines demonstrated that the cooperative effect between light and the micellar PS was consistently higher in the tumorigenic cells, particularly at higher drug concentrations and light doses, further validating the therapeutic potential of this nanocarrier system.

4.3. Mechanistic Insights and Contextualization with Prior Literature

Mechanistically and in the context of prior work, these findings are coherent with the established rationale for nano-enabled PDT strategies. Micelles improve the aqueous handling of cationic thiazine dyes such as TB, effectively suppress concentration-dependent aggregation, and can heighten local ROS yields upon red-light excitation. At the tissue scale, nanocarriers of approximately 100 nm leverage the EPR effect to preferentially accumulate in tumor tissues, a phenomenon arising from the leaky vasculature and impaired lymphatic drainage characteristic of solid tumors [29]. The literature extensively supports TB's photodynamic efficacy across various malignant and infectious models, and importantly, highlights that nanocarriers can accelerate cellular uptake and prolong intracellular retention relative to free dyes, features that map directly onto the stronger QU-DB responses observed in the present study under otherwise matched light dosing conditions. These collective observations underscore the translational potential of nanomicellar TB formulations for PDT applications in oncology.

4.4. The Multifunctional Role of Nanoparticles in Cancer Theranostics

Beyond PDT, nanoparticles have emerged as versatile platforms that simultaneously address multiple challenges in cancer diagnosis and treatment and even protection [30-32]. In the context of radiation therapy, nanoparticles incorporating high atomic number elements such as gold, platinum, or bismuth can serve as potent radiosensitizers. These nanoparticles enhance the local radiation dose through the generation of secondary electrons and Auger electrons upon X-ray irradiation, thereby amplifying DNA damage and ROS production specifically within the tumor microenvironment [33]. This radiosensitization effect effectively overcomes the inherent radioresistance of certain tumors and allows for dose reduction, consequently minimizing damage to adjacent healthy tissues. Concurrently, nanoparticles engineered with paramagnetic or superparamagnetic properties, such as gadolinium (Gd)-based agents or iron oxide nanoparticles [34], function as highly effective contrast agents for Magnetic Resonance Imaging (MRI). These nanoscale contrast agents improve the relaxivity and enhance the signal-to-noise ratio, enabling precise tumor delineation, real-time monitoring of treatment response, and accurate treatment planning for image-guided radiotherapy. This convergence of therapeutic and diagnostic functionalities within a single nanoplatform, known as theranostics, represents a paradigm shift toward personalized cancer management.

The therapeutic and diagnostic capabilities of nanoparticles align seamlessly with the objectives of the present study. Just as the TB-loaded NMs were designed to enhance selective tumor accumulation and reduce collateral damage to healthy cells through the EPR effect, radiosensitizing nanoparticles similarly exploit passive targeting mechanisms to concentrate within tumor tissues and amplify the efficacy of radiation therapy [35]. Moreover, by functioning as contrast agents, these nanoparticles enable concurrent imaging, allowing for the visualization of tumor boundaries and the assessment of treatment outcomes in real-time. This integrated approach not only enhances the precision of cancer therapy but also facilitates adaptive treatment strategies based on individual patient responses. The synergistic combination of PDT with radiotherapy, guided by MRI-based imaging, could potentially offer a comprehensive therapeutic strategy for lung cancer, addressing both the primary tumor and metastatic lesions while minimizing systemic toxicity. Therefore, the nanomicellar system developed in this study represents a foundational step toward the development of multifunctional nanoplatforms that integrate PDT, radiotherapy, and diagnostic imaging capabilities for next-generation cancer treatment [21].

Beyond PDT, nanotechnology has emerged as a transformative strategy to overcome the inherent limitations of conventional cancer treatments. Today, nanoparticles have significantly contributed to both diagnosis and therapy of malignant tissues, owing to their unique physicochemical properties, including nanoscale dimensions, high surface-to-volume ratio, tunable surface chemistry, and the ability to exploit the EPR effect for passive tumor targeting [12,14]. These versatile platforms have demonstrated outstanding performance in improving diagnostic imaging modalities, such as CT through high-atomic-number contrast agents (e.g., gold and bismuth nanoparticles) and MRI via paramagnetic or superparamagnetic agents (gadolinium-based compounds and iron oxide nanoparticles), enabling precise tumor delineation and real-time treatment monitoring [30,31]. Furthermore, nanoparticles have exhibited a superior role in enhancing the efficacy of various cancer treatment modalities, including radiotherapy (as potent radiosensitizers), chemotherapy (through targeted drug delivery and overcoming multidrug resistance), photothermal therapy (via localized hyperthermia), and PDT (by improving PS delivery and ROS generation) [28,29]. The combination of these therapeutic approaches with diagnostic capabilities within a single nanoplatform—known as theranostics—has recently gained substantial momentum, offering personalized, image-guided, and multi-modal cancer management. Among the diverse array of nanocarriers, NMs hold a distinguished position due to their remarkable ability to improve the solubility and photostability of hydrophobic or aggregating drugs, their ease of fabrication, biocompatibility, and suitability for clinical translation [13,15]. These self-assembled colloidal structures, typically composed of amphiphilic surfactants, feature a hydrophobic core for encapsulating poorly soluble agents and a hydrophilic

shell that ensures prolonged circulation and stealth properties. In this context, the nanomicellar system developed in the present study, which successfully encapsulated TB and demonstrated superior stability, enhanced ROS generation, and selective cytotoxicity in lung cancer cells, represents a foundational platform that can be further adapted for radiosensitization applications [29]. Given that TB-loaded NMs effectively reduced aggregation and improved cellular uptake in tumorigenic QU-DB cells while maintaining low toxicity in normal MRC-5 fibroblasts, this nanocarrier holds significant potential for future integration with radiosensitizing agents, thereby offering a dual-modality approach that combines PDT and radiotherapy to maximize tumor control while minimizing systemic side effects [36].

4.5. Study Limitations and Future Perspectives

Despite the encouraging results, several important limitations should be acknowledged. First, the encapsulation efficiency was moderate (36.8%), necessitating further optimization of formulation parameters such as surfactant ratio, drug-to-surfactant ratio, and processing conditions to enhance drug loading. Second, physical stability assessments revealed gradual particle growth over two weeks (PDI increase from 0.214 to 0.346), indicating that long-term storage stability requires improvement through alternative formulation strategies or lyophilization. Third, we did not evaluate empty nanomicelles (without TB) as a control group, although dark toxicity results for TB-loaded NMs were comparable to untreated controls, indirectly suggesting surfactant safety. Future studies should include empty NM controls to definitively rule out surfactant-induced cytotoxicity. Fourth, the release kinetics of TB from nanomicelles were not assessed; however, the enhanced photodynamic efficacy observed with the micellar formulation may be attributed, at least in part, to sustained drug release. We have initiated release kinetic studies using dialysis membrane methods for future investigation. Fifth, the stability of nanomicelles in complete cell culture medium containing 10% FBS was not evaluated, and protein corona formation could potentially affect NM behavior and cellular uptake. Sixth, TEM/SEM imaging was not performed to confirm morphology, although DLS analysis provided size distribution data and negative staining TEM images from an independent batch confirm spherical morphology. Seventh, and most importantly, the micellar formulation did not achieve a statistically significant improvement in selectivity index over free TB ($p = 0.22$), suggesting that passive targeting through the EPR effect is insufficient to enhance therapeutic selectivity. This finding highlights the need for active targeting strategies, such as conjugation with tumor-specific ligands (namely, folate, transferrin, or RGD peptides), or co-formulations with oxygen-shuttling agents to enhance therapeutic selectivity. Eighth, the findings are limited to in vitro experiments on two lung cell lines under normoxic conditions; future studies should extend to 3D tumor spheroid models, hypoxic conditions (to mimic tumor microenvironment), and in-vivo evaluations to confirm translational potential. Despite these limitations, the results demonstrate a clear proof-of-concept for TB-loaded nanomicelles as an effective PDT platform for lung cancer cells in-vitro.

5. Conclusion

In summary, this study successfully demonstrated that encapsulation of TB within NMs significantly enhances its physicochemical properties and photodynamic therapeutic efficacy against lung cancer cells. The nanomicellar formulation effectively protected TB against aggregation and degradation, as evidenced by superior physical stability (31% vs. 54% absorbance decline over two weeks for micellar and free forms, respectively) and favorable size distribution (40–100 nm) suitable for EPR-mediated tumor accumulation. Notably, the formulation exhibited excellent biocompatibility with minimal dark toxicity in both cancerous and normal cell lines, while demonstrating significantly enhanced photocytotoxicity against QU-DB cancer cells compared with MRC-5 normal fibroblasts under identical irradiation conditions (10, 20, and 40 J/cm²). This differential response confirms the selective therapeutic potential of the nanomicellar system. However, the moderate encapsulation efficiency (~36.8%) and lack of statistically significant improvement in selectivity index over free TB highlight areas requiring further optimization. Future directions should focus on active targeting strategies,

formulation refinement to enhance drug loading and long-term stability, and integration of diagnostic imaging capabilities to develop a multifunctional theranostic platform. Overall, TB-loaded NMs represent a promising and biocompatible nanocarrier system for PDT of lung cancer, warranting further preclinical and clinical investigations to translate this approach into clinical practice.

References

1- Amanda Leiter, Rajwanth R Veluswamy, and Juan P Wisnivesky, "The global burden of lung cancer: current status and future trends." *Nature reviews Clinical oncology,* Vol. 20 (No. 9), pp. 624–39, (2023).

2- Bagher Farhood, Behzad Raei, Reza Malekzadeh, Maryam Shirvani, Masoud Najafi, and Tohid Mortezazadeh, "A review of incidence and mortality of colorectal, lung, liver, thyroid, and bladder cancers in Iran and compared to other countries." *Contemporary Oncology/Współczesna Onkologia,* Vol. 23 (No. 1), pp. 7–15, (2019).

3- Sivapar V Mathan, Mohit Rajput, and Rana P Singh, "Chemotherapy and radiation therapy for cancer." in *Understanding cancer*: *Elsevier*, (2022), pp. 217–36.

4- Dennis EJGJ Dolmans, Dai Fukumura, and Rakesh K Jain, "Photodynamic therapy for cancer." *Nature reviews cancer,* Vol. 3 (No. 5), pp. 380–87, (2003).

5- A Ferreira Dos Santos, DR Queiroz de Almeida, Leticia Ferreira Terra, Maurício S Baptista, and Leticia Labriola, "Photodynamic therapy in cancer treatment-an update review." *J. cancer metastasis Treat,* Vol. 5 (No. 25), p. 10.20517, (2019).

6- Omid Talaee *et al.*, "Characterization of a HER-2 targeted silica-gold nanoshells for breast cancer radio-photothermal therapy." *Applied Radiation and Isotopes,* p. 112454, (2026).

7- Tae Eun Kim and Ji-Eun Chang, "Recent studies in photodynamic therapy for cancer treatment: from basic research to clinical trials." *Pharmaceutics,* Vol. 15 (No. 9), p. 2257, (2023).

8- Stefan W Ryter *et al.*, "Mechanisms of cell death in oxidative stress." *Antioxidants & redox signaling,* Vol. 9 (No. 1), pp. 49–89, (2007).

9- Srivalleesha Mallidi, Sriram Anbil, Anne-Laure Bulin, Girgis Obaid, Megumi Ichikawa, and Tayyaba Hasan, "Beyond the barriers of light penetration: strategies, perspectives and possibilities for photodynamic therapy." *Theranostics,* Vol. 6 (No. 13), p. 2458, (2016).

10- Mohammad Ali Mozayeni, Farzaneh Vatandoost, Mohammad Asnaashari, Mehdi Shokri, Saranaz Azari-Marhabi, and Negin Asnaashari, "Comparing the efficacy of toluidine blue, methylene blue and curcumin in photodynamic therapy against Enterococcus faecalis." *Journal of lasers in medical sciences,* Vol. 11 (No. Suppl 1), p. S49, (2020).

11- Benedicto de Campos Vidal and Maria Luiza S Mello, "Toluidine blue staining for cell and tissue biology applications." *Acta histochemica,* Vol. 121 (No. 2), pp. 101–12, (2019).

12- Lama Misba, Shatavari Kulshrestha, and Asad U Khan, "Antibiofilm action of a toluidine blue O-silver nanoparticle conjugate on Streptococcus mutans: a mechanism of type I photodynamic therapy." *Biofouling,* Vol. 32 (No. 3), pp. 313–28, (2016).

13- Bahman Alipour *et al.*, "Advances in nano-scale metal-based contrast agents for computed tomography: a systematic review." *Radiation Physics and Chemistry,* Vol. 226p. 112195, (2025).

14- Yasin Ayyami, Marjan Ghorbani, Masoumeh Dastgir, Reza Malekzadeh, and Tohid Mortezazadeh, "Chitosan-modified manganese oxide-conjugated methotrexate nanoparticles delivering 5-aminolevulinic acid as a dual-modal T1–T2* MRI contrast agent in U87MG cell detection." *Magnetic resonance materials in physics, biology and medicine,* Vol. 37 (No. 5), pp. 909–24, (2024).

15- Masoumeh Dastgir *et al.*, "Synergistic radiosensitization of breast cancer using bismuth oxide nanoparticles coated with chitosan and β-cyclodextrin loaded with curcumin and 5-aminolevulinic acid." *Cancer Nanotechnology,* Vol. 17 (No. 1), p. 8, (2026).

16- Reza Malekzadeh *et al.*, "Dose enhancement by gold, iron oxide, bismuth oxide, and platinum nanoparticles in radiotherapy: a comprehensive meta-analysis." *Radiological Physics and Technology,* Vol. 19 (No. 2), pp. 479–98, (2026).

17- Haniye Ahrabi *et al.*, "Dual-Purpose 5-Aminolevulinic Acid-Loaded Iron Oxide Nanoparticles: Enhancing Radiotherapy and MRI in Glioblastoma." *Journal of Drug Delivery Science and Technology,* p. 107853, (2025).

18- Yasin Ayyami *et al.*, "Characterization and application of targeted MnO2/CS@ ALA-MTX nano-radiosensitizers for boosting X-ray radiotherapy of brain tumors." *Colloids and Surfaces A: Physicochemical and Engineering Aspects,* Vol. 692p. 133975, (2024).

19- Maedeh Yektamanesh, Yasin Ayyami, Marjan Ghorbani, Masoumeh Dastgir, Reza Malekzadeh, and Tohid Mortezazadeh, "Characterization of multifunctional β-cyclodextrin-coated Bi2O3 nanoparticles conjugated with curcumin for CT imaging-guided synergetic chemo-radiotherapy in breast cancer." *International Journal of Pharmaceutics,* Vol. 659p. 124264, (2024).

20- Reza Malekzadeh *et al.*, "Nanoarchitecture-based photothermal ablation of cancer: a systematic review." *Environmental research,* Vol. 236p. 116526, (2023).

21- Salah M Tawfik, Shavkatjon Azizov, Mohamed R Elmasry, Mirkomil Sharipov, and Yong-Ill Lee, "Recent advances in nanomicelles delivery systems." *Nanomaterials,* Vol. 11 (No. 1), p. 70, (2020).

22- Hoang M Trinh, Mary Joseph, Kishore Cholkar, Ranjana Mitra, and Ashim K Mitra, "Nanomicelles in diagnosis and drug delivery." in *Emerging nanotechnologies for diagnostics, drug delivery and medical devices*: *Elsevier*, (2017), pp. 45–58.

23- Haniye Ahrabi, Reza Malekzadeh, and Ghazale Geraily, "Application of 5-aminolevulinic acid in cancer radio-dynamic therapy: A systematic review." *Radiation Physics and Chemistry,* Vol. 236p. 112910, (2025).

24- Hua Guo, Huimin Wang, Hong Deng, Yiyi Zhang, Xue Yang, and Weiqi Zhang, "Facile preparation of toluidine blue-loaded DNA nanogels for anticancer photodynamic therapy." *Frontiers in Bioengineering and Biotechnology,* Vol. 11p. 1180448, (2023).

25- KM Gangotri, RC Meena, and Rajni Meena, "Use of micelles in photogalvanic cells for solar energy conversion and storage: cetyl trimethyl ammonium bromide-glucose-toluidine blue system." *Journal of Photochemistry and Photobiology A: Chemistry,* Vol. 123 (No. 1-3), pp. 93–97, (1999).

26- Reza Malekzadeh, Behnaz Babaye Abdollahi, Marjan Ghorbani, Jalil Pirayesh Islamian, and Tohid Mortezazadeh, "Trastuzumab conjugated PEG–Fe3O4@ Au nanoparticle as an MRI biocompatible nano-contrast agent." *International Journal of Polymeric Materials and Polymeric Biomaterials,* Vol. 72 (No. 10), pp. 759–70, (2023).

27- Ana-Maria Vlasceanu, Daniela L Baconi, Bianca Galateanu, Miriana Stan, and Cristian Balalau, "Comparative cytotoxicity study of nicotine and cotinine on MRC-5 cell line." *Journal of Mind and Medical Sciences,* Vol. 5 (No. 1), p. 17, (2018).

28- Alwan Al-Qushawi *et al.*, "Preparation and characterization of three tilmicosin-loaded lipid nanoparticles: physicochemical properties and in-vitro antibacterial activities." *Iranian Journal of Pharmaceutical Research: IJPR,* Vol. 15 (No. 4), p. 663, (2016).

29- Xiaoxiao Gu, Haoyang Yuan, Cailing Li, Lixian Xu, Shuang Li, and Dinghua Yu, "Toluidine blue O photosensitizer combined with caffeic acid improves antibacterial performance by increasing the permeability of cell membrane." *Colloids and Surfaces B: Biointerfaces,* Vol. 233p. 113657, (2024).

30- Parinaz Mehnati, Reza Malekzadeh, and Sooteh Mohammad Yousefi, "New Bismuth composite shield for radiation protection of breast during coronary CT angiography." (2019).

31- Parinaz Mehnati, Reza Malekzadeh, Mohammad Yousefi Sooteh, and Soheila Refahi, "Assessment of the efficiency of new bismuth composite shields in radiation dose decline to breast during chest CT." *The Egyptian Journal of Radiology and Nuclear Medicine,* Vol. 49 (No. 4), pp. 1187–89, (2018).

32- Nikan Asadpour, Reza Malekzadeh, Saeed Rajabpour, Soheila Refahi, Parinaz Mehnati, and Ahmad Shanei, "Shielding performance of multi-metal nanoparticle composites for diagnostic radiology: an MCNPX and Geant4 study." *Radiological Physics and Technology,* Vol. 16 (No. 1), pp. 57–68, (2023).

33- Behnaz Babaye Abdollahi *et al.*, "Main approaches to enhance radiosensitization in cancer cells by nanoparticles: A systematic review." *Advanced pharmaceutical bulletin,* Vol. 11 (No. 2), p. 212, (2020).

34- Hedieh Mansouri *et al.*, "A biocompatible theranostic nanoplatform based on magnetic gadolinium-chelated polycyclodextrin: in vitro and in vivo studies." *Carbohydrate polymers,* Vol. 254p. 117262, (2021).

35- Junjie Liu, Jinjin Shi, Weimin Nie, Sijie Wang, Genhua Liu, and Kaiyong Cai, "Recent progress in the development of multifunctional nanoplatform for precise tumor phototherapy." *Advanced healthcare materials,* Vol. 10 (No. 1), p. 2001207, (2021).

36- Lama Misba, Hayder Abdulrahman, and Asad U Khan, "Photodynamic efficacy of toluidine blue O against mono species and dual species bacterial biofilm." *Photodiagnosis and Photodynamic Therapy,* Vol. 26pp. 383–88, (2019).